arXiv:1402.3509v1 [astro-ph.GA] 14 Feb 2014

Determining Inclinations of Active Galactic Nuclei Via Their Narrow-Line Region Kinematics - II. Correlation With Observed Properties [1]

T.C. Fischer[2], D.M. Crenshaw[2], S.B. Kraemer[3], H.R. Schmitt[4], T.J. Turner[5]

ABSTRACT

Active Galactic Nuclei (AGN) are axisymmetric systems to first order; their observed properties are likely strong functions of inclination with respect to our line of sight, yet the specific inclinations of all but a few AGN are generally unknown. By determining the inclinations and geometries of nearby Seyfert galaxies using the kinematics of their narrow-line regions (NLRs), and comparing them with observed properties, we find strong correlations between inclination and total hydrogen column density, infrared color, and Hβ full-width at half maximum (FWHM). These correlations provide evidence that the orientation of AGN with respect to our line of sight affects how we perceive them, beyond the Seyfert 1/2 dichotomy. They can also be used to constrain 3D models of AGN components such as the broad-line region and torus. Additionally, we find weak correlations between AGN luminosity and several modeled NLR parameters, which suggests that the NLR geometry and kinematics are dependent to some degree on the AGN's radiation field.

Subject headings: galaxies: active, galaxies: Seyfert, galaxies: kinematics and dynamics, galaxies: individual(Circinus, Mrk 34, Mrk 279, Mrk 1066, NGC 1667, NGC 3227, NGC 3783, NGC 4051, NGC 4507, NGC 5506, NGC 5643, NGC 7674)

---

[1]Based on observations made with the NASA/ESA Hubble Space Telescope, obtained at the Space Telescope Science Institute, which is operated by the Association of Universities for Research in Astronomy, Inc. under NASA contract NAS 5-26555. These observations are associated with programs 11243, 11611, and 12212

[2]Department of Physics and Astronomy, Georgia State University, Astronomy Offices, 25 Park Place, Suite 600, Atlanta, GA 30303; fischer@chara.gsu.edu

[3]Institute for Astrophysics and Computational Sciences, Department of Physics, The Catholic University of America, Washington, DC 20064

[4]Naval Research Laboratory, Washington, DC 20375

[5]Department of Astronomy, University of Maryland, College Park, MD 20742

1. Introduction

Seyfert galaxies represent a relatively moderate luminosity ($L_{bol} \approx 10^{43} - 10^{45}$ erg s^{-1}), nearby (z $\leq$ 0.1) subset of the overall collection of AGN, which exhibit a dichotomy of broadened and unbroadened permitted emission lines. This dichotomy has led the Seyfert class of AGN to be divided into two groups (Khachikian & Weedman 1974), with Seyfert 1s exhibiting spectra containing broad (full width at half-maximum [FWHM] $\geq$ 1000 km s^{-1}) permitted lines, narrower (FWHM $\leq$ 1000 km s^{-1}) forbidden lines, and distinct, non-stellar optical and UV continua, and Seyfert 2s containing only narrow permitted and forbidden emission lines, with their optical and UV continua being dominated by the host galaxy.

Osterbrock (1978) suggested that Seyfert 1s and 2s were physically the same objects, but that the BLRs of Seyfert 2s are obscured along our line of sight (LOS). The strongest observational evidence for a unified model stems from work by Antonucci & Miller (1985), who discovered that weak, polarized broad emission lines do exist in Seyfert 2 galaxies by analyzing the polarized spectrum of the Seyfert 2 NGC 1068. This observation led to the generation of a unified AGN model, with AGN being similar objects, obscured by a toroidal structure of gas and dust in Seyfert 2s (Antonucci 1993), viewed from different angles. Observing an AGN from near the axis of the torus would allow for the viewing of the central source, the BLR, and the NLR, and produce the spectrum of a Seyfert 1, while observing the same AGN from near the plane of the torus would leave only the NLR and a small amount of emission from the nuclear source visible, producing a Seyfert 2 spectrum. It is important to note that this is an oversimplified scenario, in which each AGN with a given luminosity is contained within an identical, smooth-density torus. In reality, the torus around each AGN likely varies in covering factor, or how much sky at the AGN center is covered by obscuring material, and has a clumpy composition that does not create a hard cut-off between observing a Type 1 or Type 2 AGN, but instead only reduces the probability to directly view the AGN as our line of sight strays further from the torus axis (Elitzur 2012). The NLR is then the radiation that has escaped the torus, forming a biconical structure likely governed by the torus covering factor, with an axis that is perpendicular to the plane of the torus.

In our previous paper (Fischer et al. 2013, henceforth Paper I), we measured radial velocities of [O III] emission knots across NLRs for 47 Seyfert AGN observed with *Hubble Space Telescope* (*HST*) STIS G430L/M gratings. From our measurements, 12 AGN showed clear evidence for kinematics dominated by biconical outflow, where knots accelerated out from the inner nucleus, reached a terminal velocity, and then decelerated back toward the AGN systemic velocity. In order to determine the geometry, including the inclination of their NLR outflows, and thus the inclination of their torus, (both of which generally unknown for all but a few AGN) a kinematic model was fit to the observed NLR kinematics using a simple,

linear velocity law. Using available imaging and kinematic data for each AGN to create an initial geometry, we refined the model in an iterative process until a best fit to the kinematic data was obtained. Including 5 AGN previously modeled by our group (Crenshaw et al. 2000; Crenshaw & Kraemer 2000; Ruiz et al. 2001; Das et al. 2005, 2006; Crenshaw et al. 2010b; Fischer et al. 2010, 2011), we now have an initial sample of 17 AGN inclinations, from which we can begin to determine how their observed properties vary as a function of polar angle (i.e. the inclination of the torus) with respect to the accretion disk and/or torus axes, and identify correlations that probe the structure of the AGN components by comparing our kinematic model results with observed multiwavelength properties of these AGN.

Section 2 describes the parameters and how they were measured. Section 3 illustrates all relevant comparisons between modeled and observed AGN parameters. Sections 4 notes significant non-correlations. Section 5 contains discussion and final conclusions.

2. Parameters

2.1. Kinematic Model Parameters

Our kinematic models employed in Paper I, combined several basic input parameters to generate a 3D biconical NLR which simulated the deprojected outflow velocities as a function of radius from the AGN. To review, the parameters and their definitions are as follows. Position angle ($P.A.$) is the angle between North and the bicone axis in the plane of the sky, measured in the eastward (counter-clockwise) direction. Inclination (i) of the bicone is measured out of the plane of the sky, such that $i = 0$ places the bicone axis in the plane of the sky and $i = 90$ places the bicone axis parallel to our line of sight. Inner and outer opening angles (θ_{min},θ_{max}) are angles between the bicone axis and the inner and outer edges of the bicone model respectively. Our model includes an inner opening angle as previous NLR outflow studies have shown a lack of low velocity kinematic measurements near the peaks of the kinematic curves, which suggests that the NLR is often evacuated of [O III] emission along its axis. Maximum velocity (v_{max}) is the boundary value set in the model velocity law $v = kr$, where velocity increases with radius until the maximum velocity is reached at the turnover radius (r_t) then decreases linearly to zero. Maximum height (z_{max}) is the distances from the nucleus to one end of the bicone, measured along the bicone axis. Model parameters are initially set to observed values via imaging and spectroscopy and altered in an iterative process until the model agrees with the kinematic data. All values are deprojected (i.e. corrected for inclination). Final parameters for each modeled AGN are listed in Table 1.

2.2. Physical Properties

To determine how NLR geometry might be correlated with observable parameters of AGN, we gathered measurements from the literature, and in a few cases our own observations, of several observed AGN properties likely to be affected by viewing angle with respect to the NLR bicone axis and/or torus inclination, which we designate as polar angle (or torus inclination) $\theta = 90^\circ - i$, where i is the inclination of the bicone axis out of the plane of the sky. These properties include total hydrogen column density in the line of sight to the nucleus (N_H), mid-IR color defined by continuum flux ratios from *Spitzer* observations, and full-width at half-maximum (FWHM) of $H\beta$ emission from the broad-line region. We list the observed and physical properties and their uncertainties in Table 2.

Bolometric luminosities were obtained by integrating across all available spectral energy distribution (SED) flux points (Woo & Urry 2002) or derived from [O III] ($log(L_{Bol}) \approx log(L_{[OIII]}) + log(3500)$; Heckman et al. 2004, 2005; Meléndez et al. 2008) or 2-10 keV X-ray (Malaguti et al. 1998) luminosities. Super-massive black hole (SMBH) masses of Seyfert 1 AGN were determined using reverberation mapping, where BLR size, estimated from the time lag between corresponding ionizing continuum and broad line emission fluxes, and broad-line velocities are combined to calculate the AGN black hole mass (Peterson et al. 2004; Bentz et al. 2006; Denney et al. 2009, 2010). SMBH masses for Seyfert 2s Circinus and NGC 1068 were gathered employing direct, dynamical mass-measurements (Greenhill et al. 2003; Lodato & Bertin 2003). Remaining Seyfert 2 AGN SMBH masses were indirectly constrained utilizing stellar velocity dispersions as they correlate well with black holes masses determined from spatially resolved kinematics (Tremaine et al. 2002).

Type 2 AGN neutral column densities are measured directly through X-ray observations. As the column density of material, containing mostly hydrogen, within the obscuring torus surrounding the AGN increases, more ionizing radiation is absorbed. This effect can be prominently observed in the X-ray using the *Chandra*, *XMM-Newton*, and *Suzaku* observatories, where emission from an obscured AGN is absorbed below a specific energy due primarily to the H and He edges (Turner & Miller 2009). The emission that remains is fit with an absorbed power law model to determine N_H (Winter et al. 2009). Values with lower limits are due to X-ray absorption extending to energies higher than could be observed by a specific observatory, which could therefore not be fit with a power law. In cases where the absorber is Compton thick, the lower limit is $N_H \approx 10^{24}$ to 10^{25} cm^{-2}, depending on the observations. For Seyfert 2s, we assume that the total hydrogen column density in the line of sight to the nucleus is dominated by the neutral gas, i.e. $N_H \approx N_{HI}$.

For Type 1 AGN, where we can assume that we are looking into the inner portion of the AGN (as verified in Paper I), we do not observe large neutral hydrogen column densities

representative of the material found in the torus surrounding the central engine. Instead, we typically measure ionized column densities from "AGN winds" (Crenshaw et al. 2003), generally seen in the X-ray but have also been traced in the UV (Crenshaw & Kraemer 2012), and determine N_H from photoionization models. In short, intensities of two or more resonance doublet line species (e.g. C IV, N V) are measured which allow for the calculation of the covering factor of the outflowing absorbers with respect to the background emission, which in turn allows for the calculation of the optical depth of each absorption feature. The ionic column density of each absorption line is then obtained by integrating the optical depth across the line profile (Crenshaw et al. 2003). These ionic column densities are used to determine the ionization parameter (ratio of ionizing photon density to gas density, U) and N_H $(= N_{HI} + N_{HII})$ via CLOUDY photoionization modeling (Kraemer et al. 2009, 2012). The listed N_H values for each Sy 1 in our sample are the summed column densities across all absorption components. Uncertainties in the column densities for both Seyfert 1s and 2s are from the model uncertainties in the original references. For cases with multiple values, due to variability for example, we used an average value and standard deviation for the column densities and their uncertainties.

For the Seyfert 1 galaxies, we include the UV and X-ray "warm absorbers" (Crenshaw & Kraemer 2012), but not the highly-ionized ultra-fast outflow (UFO) absorbers detected in the Fe K-shell absorption lines, because the two types are quite distinct in terms of ionization parameter, outflow velocity, distance from the central AGN, and column density (Tombesi et al. 2013, and references therein). UFOs may therefore represent a physically distinct component of AGN, whereas a strong connection has already been established between the UV and X-ray warm absorbers (Crenshaw et al. 2003). We will include the high-ionization absorbers (at all outflow velocities) in a future study to investigate their dependence on inclination and possible connection to the warm absorbers.

We retrieved mid-IR spectra from the Cornell Atlas of Spitzer/IRS Sources (CASSIS) (Lebouteiller et al. 2011), which provides reduced low-resolution spectra ($R \sim 60 - 127$ over 5.2μm to 38μm) taken by the Infrared Spectrograph (IRS) instrument aboard *Spitzer*. Spectra were extracted through a dedicated pipeline from which we chose a regular "tapered" extraction suggested for extended sources. Measuring continuum fluxes over small bins at 5.5μm, 13.7μm, 20μm, and 30μm (shown in Figure 1) allowed us to determine the mid-IR color of each AGN. Each observation was obtained in four segments that required scaling before each segment was combined into a single spectrum. Segments were scaled such that overlapping ends of each segment were equal in flux, creating a continuous spectrum when combined. As we are interested in relative fluxes, accurate absolute flux values are not a concern.

The FWHM of the broad component of Hβ in each Seyfert 1 was obtained from the literature or our own observations. Observations of NGC 3227 were obtained using the DeVeny spectrograph on the 1.8m Perkins telescope at the Lowell Observatory in Flagstaff, Arizona. Spectra were taken on 2010 December 9 using a slit width of 2″ for a total exposure of 1200s and dispersed into spectral images using the 'blue' 300 line mm^{-1} grating with a resolving power of ∼2145 (∼140 km s^{-1}).Observations for NGC 3783 was obtained using the R-C spectrograph on the 1.5 SMARTS telescope at the Cerro Tololo Inter-American Observatory (CTIO) in La Serena, Chile. Long-slit spectra were taken on 2003 April 25 for a total exposure time of 1800s using the 600 line mm^{-1} '#26' grating with a resolving power of ∼1165 (∼257 km s^{-1}). Both sets of observations were reduced two-dimensionally using their respective IRAF packages and collapsed to a single spectrum, resulting in wavelength calibrated spectra in flux units from which FWHMs could be measured.FWHM measurements for the remaining targets were obtained from the literature from studies using similar techniques, which included the removal of the narrow component of Hβ. We estimate our uncertainties in FWHM by using different reasonable continuum placements and estimates for the narrow Hβ fluxes, which typically result in percentage errors of 10%.

Molecular hydrogen masses (M_{H_2}) were estimated via K-band IFU observations from SINFONI and OSIRIS by Müller Sánchez et al. (2009); Hicks et al. (2009)and Friedrich et al. (2010). In these studies, Gaussians were fit to the bright 1-0 S(1) molecular hydrogen line at 2.1218 μm across the inner 30 pc of each AGN to measure the rotational velocity of the system and calculate a dynamical mass within that radius, using the assumption that the gas is in a disk-like distribution around the AGN, from which a molecular hydrogen gas mass was estimated using a typical gas mass fraction of 10%. Masses listed for Circinus and NGC 1068 are not included in our correlation analysis as the mass estimation for Circinus was only done for the inner 9 pc of the AGN and the mass in NGC 1068 may be miscalculated as the inflowing H_2 kinematics do not conform to the rotational pattern seen in other AGN. NGC 3227 was observed by both listed instruments and thus the average between the two mass estimates is used.

3. Correlations

Using the kinematic modeling results from Paper I, we have the opportunity to compare geometrical aspects of the AGN NLRs to their other observed physical properties in order to detect any correlations between them for the first time. Table 3 lists the correlations examined, their resultant correlation coefficient r, the sample size N, and the probability (or p-value) of exceeding r using a random sample of N observations taken from an uncorrelated

parent population $P_c(r, N)$. A p-value $< 5\%$ indicates a statistically significant correlation that is highly unlikely to be observed under a null hypothesis. The maximum sample size is one less than our total AGN sample size, as we omit NGC 5506 from our comparisons, as explained in Section 4.

3.1. Inclination

We can determine how observed AGN properties vary as a function of polar angle with respect to the accretion disk and/or torus axes by comparing them to the modeled inclinations in our AGN sample. The unified model of AGN posits the presence of a torus surrounding the AGN where the central engine and source of broad line emission is visible in Type 1 AGN and obstructs our view to the central engine in Type 2 targets.

Figure 2 compares column density N_H against the polar angle θ $(= 90 - i)$ of the bicone axis for each of our modeled AGN. Including both types of Seyferts, there is a distinct correlation between the two parameters, where observing an AGN further from the axis of its NLR and closer to the plane of the toroidal structure corresponds to a increased neutral hydrogen column density along our line of sight to the central engine. By removing NGC 5506 (an alteration kept for the remainder of this work), and Mrk 279, as column densities from several its absorbers have yet to be determined (Crenshaw & Kraemer 2012), we calculate a coefficient of $r = 0.86$, which corresponds to a p-value of $P_c(r, N) < 0.01\%$, indicating that as our line of sight with respect to the bicone axis (polar angle) increases, the torus surrounding the AGN becomes closer to edge-on and we see an increase in column densities for both Seyfert 1s and Seyfert 2s. Seyfert 1s and 2s can reside at similar inclinations depending on whether or not our line of sight intersects the obscuring torus surrounding the AGN. Surprisingly, there appears to be a seamless transition in N_H between the Seyfert 1 ionized gas columns and Seyfert 2 neutral columns. As we expected the total hydrogen column (N_H) in Seyfert 2s would be dominated by neutral hydrogen and Seyfert 1s show large columns of ionized gas that dominate N_H (Crenshaw et al. 1999), this correlations suggests a possible connection between the torus and the outflowing winds of ionized gas.

Deo et al. (2009) analyzed mid-infrared (mid-IR) spectra of Seyfert galaxies using archival *Spitzer Space Telescope* observations in order to characterize the nature of the mid-IR active nuclear continuum, which is dominated by dust emission. They found that Seyfert 2s typically have weaker short-wavelength (5.5 - 14.7 μm) nuclear continua than comparable Seyfert 1s, which suggests a relationship between the mid-IR flux ratio ($F_{5\mu m}/F_{30\mu m}$)and inclination, as short-wavelength mid-IR emission is likely absorbed to a certain degree in Type 2 objects by the obstructing torus surrounding the AGN. According to the unified model,

as our view becomes more pole-on, the 5 μm emission should increase as we see more of the hot, inner throat of the torus. Comparing our results with Deo et al. (2009) for targets that are contained in both their sample and CASSIS (Mrk 3, NGC 4151, NGC 4507), we find our measured fluxes to be consistent to within 10%. As observations of certain sample AGN were not available in CASSIS, we then use flux ratios from Deo et al. (2009) for NGC 1667, NGC 4051, and NGC 7674.

Figure 3 shows a negative correlation between mid-IR color and polar angle with a correlation coefficient of $r = -0.61$ ($P_c(r, N) = 1.2\%$), supporting the idea that a smaller polar angle allows for a better view of the hot inner 'throat' of the obscuring torus. Removing NGC 3227, a Seyfert 1 galaxy known to be heavily reddened by its host galaxy (Crenshaw & Kraemer 2001), increases the correlation to $r = -0.74$ ($P_c(r, N) = 0.16\%$).

By observing the FWHM of broad Hβ emission-lines in Sy 1 targets and comparing them with their modeled inclinations, we may gain a better understanding of the BLR kinematics. Figure 4 shows a positive correlation ($r = 0.94, P_c(r, N) = 1.7\%$) between broad H$\beta$ FWHM and polar angle, despite the small number of data points, which suggests a non-spherical component to the BLR kinematics. If the BLR kinematics contain a strong rotational component, as suggested by a number of studies (Murray & Chiang 1997; Gaskell 2000, 2009), this correlation suggests that pole-on and near pole-on AGN contain velocities that may be underestimated. Thus, using the mass relation via reverberation mapping (Peterson 1997), $M = f\frac{R\Delta V^2}{G}$ where R is the size of the BLR, ΔV is the emission line width, and f is a scale factor of order unity dependent on the inclination of the BLR, amongst other things, the correlation also suggests that black-hole masses may be underestimated in some AGN (Collin et al. 2006). Although this correlation is suggestive, it cannot be used directly because the FWHM is also dependent on black hole mass and size of the BLR.

3.2. Luminosity

In addition to several observed parameters correlating with AGN inclination, we also found that several *model* parameters, r_t, v_{max}, and z_{max}, each exhibit a possible positive correlation with AGN bolometric luminosity. Figures 5-7 suggest that as the AGN increases in luminosity, the maximum values of these parameters also increase. Correlations of v_{max} and r_t with luminosity suggest that radiative driving is an important factor within the NLR. As luminosity increases, the increased number of photons accelerate gas clouds in the NLR to higher velocities out to further distances before decelerating. The increased number of photons also continue to ionize gas further from the nucleus, increasing the total NLR bicone height. However, the correlations provided are very weak, so much so that comparing z_{max}

with luminosity results in a p-value of $P_c(r, N) > 5\%$, which indicates that the correlation is not statistically significant. Modeled NLR geometries for additional AGN are required before these relations can be further analyzed.

Additionally, we find a strong ($P_c(r, N) = 0.01\%$) correlation between bicone height and kinematic turnover radius (Figure 8), which suggests that geometric and kinematic scales are related, likely via AGN luminosity.

4. Non-Correlations

Through the Unified Model, the central engine is obstructed by an optically thick disk (Antonucci 1993) such that a majority of the ionizing radiation is collimated into a biconical structure that has been observed to vary in opening angle amongst different AGN (Schmitt et al. 2003). As such, any correlations including the NLR opening angle may provide information about the composition of the surrounding torus. However, of all the intrinsic NLR model parameters (i.e. not inclination or position angle), outer opening angle appears to be highly uncorrelated with both observed and modeled AGN properties in our sample, as shown by the high $P_c(r, N)$ values for correlations with θ_{max} in Table 3. These results disagree with previous correlations found by Müller-Sánchez et al. (2011) using similar NLR modeling techniques, where opening angle, maximum outflow velocity, and molecular hydrogen mass within the inner torus, each appeared dependent on one another, indicating that more massive tori restrict NLRs from expanding in opening angle and produce higher velocity outflows. Some of the discrepancy may be that we do not have enough dynamic range as our molecular mass comparisons contain a very small sample size of four AGN. However, we are able to compare outflow velocity and opening angle for our entire sample and find little correlation between these two parameters.

5. Discussion and Conclusions

With inclinations and geometries of 17 Seyfert galaxies, our model results suggest that Seyfert 1 AGN are inclined further toward our LOS than Seyfert 2 AGN. Knowing the inclinations of these AGN allows us to determine how their observed properties vary as a function of polar angle with respect to the accretion disk and/or torus axes. We have established a strong connection between polar angle and column density, which probes the structure of the obscuring torus, the ionized gas outflows, and the connection between the two; polar angle and broad Hβ FWHM, suggesting a non-spherical component to the BLR

kinematics; and polar angle and mid-IR color (5 μm/30 μm flux), presumably indicating a better view of the hot inner "throat" of the obscuring torus in Seyfert 1s compared to Seyfert 2s.

With the discovery of three independent correlations on inclination, we can see that our line of sight affects how we observe specific parameters of our sample and thus that the obstructing torus surrounding the central engine plays a significant role in how we observe these AGN. Additionally, we find correlations between AGN luminosity and the NLR kinematics and geometry, but not between opening angle, molecular hydrogen mass surrounding the torus and the NLR kinematics and geometry.

Our inclination results agree with and help quantify the unified model, as N_H, IR color, and $H\beta_{FWHM}$ measurements each show a strong correlation with viewing angle. These results can thus provide valuable constraints on specific torus models (e.g. Fritz et al. 2006; Ramos Almeida et al. 2009; Roth et al. 2012; Stalevski et al. 2012) and BLR models (e.g. Collin et al. 2006; Denney 2012; Pancoast et al. 2012).

Establishing accurate, continuous correlations between AGN inclination and independent, observable parameters may allow us to use these comparatively simple to obtain observational measurements in the future as a proxy for inclination in AGN with unmodelable kinematics. What other observable parameters could be related to inclination? Could the amount of polarized light depend on inclination? As Antonucci (1993) observed, polarization of type 1 galaxies tends to be parallel to the AGN jet axis and polarization of type 2 galaxies tends to be perpendicular to the jet axis. Could this also apply to the torus axis, such that a correlation between increasing perpendicular polarization and polar angle exists?

One parameter that certainly requires further investigation is the role of the host galaxy in obscuring the AGN. As mentioned earlier, the maximum sample size is one less than our total AGN sample size, as we omit NGC 5506[1] from our comparisons because it contains a highly inclined (76°) host disk. Imaging depicts the NLR as a single cone near perpendicular to the host disk, and in Paper I, we modeled the polar angle of the NLR to be 80° from LOS. However, it is unknown how much of the visible NLR is extinguished due to the host disk orientation, although X-ray observations of NGC 5506 have shown that at least a portion of the NLR is extinguished as X-ray emission from a second NLR cone can be clearly detected on the opposite side of the nucleus from the visible NLR (Zeng 2009). As we found no correlation

[1]Paper I stated that the classification of NGC 5506 was contested, with labels of Narrow-Line Seyfert 1 (NLS1;Nagar et al. 2002) / Sy 1.9 (Maiolino & Rieke 1995) / Sy 2 AGN (Trippe et al. 2010) all being used to describe the AGN. However, Trippe et al. (2010) notes that the alternate labels do not correspond to what is seen optically in NGC 5506 and we have removed the other labels from contention in our analysis.

between NLR and host disk orientation in Paper I, it is possible that the near edge-on host disk would play a major role in obscuring portions of a moderately inclined NLR, and the interpretation of only the unobscured kinematics would thus affect the resultant kinematic model. If the NLR were to be inclined only 40 degrees from our LOS, per Fe Kα analysis in Guainazzi et al. (2010), then the NLR may be opened wide enough that a portion of the NLR intersects with the disk. Several other modeled AGN experience intersections between the host and NLR (i.e. Mrk 3, Mrk 34, Mrk 573) which illustrate that the NLR is radiation bound in an intersection scenario and emission near this intersection does not continue to radially progress through the host disk. As such, an observer near the edge of the host disk of each of these AGN would likely be unable to observe an integral portion of the NLR kinematics. Additionally, while host disks likely play a role in the amount of NLR emission that is extinguished in each AGN, they do not contain hydrogen column densities significant enough to account for the X-ray/UV absorption observed over each AGN. Comparing host disk inclination to hydrogen column density in our sample results in a correlation coefficient of $r = 0.034$ and a corresponding p-value of $P_c(r, N) = 89\%$. Thus, at its current NLR orientation, NGC 5506 has a hydrogen column density orders of magnitude lower than all other AGN at high inclinations, implying that it should have an inclination closer to our LOS. A polar angle of $\theta = 40^\circ$ would place the $N_H = 2 \times 10^{22}$ column density measurement much closer to the given correlation.

Within our limited range of luminosities, we find that outflow velocity, NLR height, and turnover radius each appear to be influenced by the luminosity of the AGN. Additionally, NLR height and turnover radius are well correlated, which means whatever is determining the ultimate reach of photons from the AGN also has some role in the dynamics of the system, extending the acceleration of NLR clouds to further distances. Could these relations provide insight on the origin of the NLR? If the NLR emitting gas primarily originates from a stream of ionizing radiation unleashed upon the galaxy, ionizing and accelerating ambient material that it encounters, the one property that should affect the geometry of the NLR the greatest would be AGN luminosity. To more properly understand this relation requires additional models to further constrain the strength of the given correlations and further study of the orientation between the NLR radiation and the plane of the host galaxy. AGN that display such an intersection (i.e. Mrk 78, NGC 4151) typically result in a more extended NLR and are more likely to host in situ acceleration of NLR gas (Fischer et al. 2010).

From our relation between bolometric luminosity and maximum outflow velocity, we see that outflow kinematics possibly cease at $L_{bol} < 10^{41}$ erg s^{-1}. *HST* STIS Hα studies similar to our own in Walsh et al. (2008) depict observed low-ionization nuclear emission-line regions (LINERs), AGN with luminosities generally lower than Seyferts, containing possible rotation (or 'ambiguous'; see Paper I) kinematics with blueshifted velocities < 250 km s^{-1}. Though

these velocities may be due to projected outflows, they could instead be a combination of rotation and ionization via star formation or post-AGB stars (Yan & Blanton 2012).

Finally, we note that although the correlations that we found are intriguing, they are based on a small number of data points. More confirmations of radial outflows in AGN and corresponding kinematic models would result in more inclinations for testing these correlations. More observations of Seyfert 2s at higher X-ray energies would help replace lower limits on N_H with actual values and additional X-ray observations of our current sample over several epochs would allow us to determine if and how much N_H varies over time.

6. Acknowledgments

TCF thanks M.C. Bentz, H.R. Miller, R.J. White, and P.J. Wiita for the useful discussions and A. Michel for aiding in Hβ FWHM measurements. The authors would also like to thank the anonymous referee for their practical suggestions which led to a much improved discussion. Some of the data presented in this paper were obtained from the Mikulski Archive for Space Telescopes (MAST). STScI is operated by the Association of Universities for Research in Astronomy, Inc., under NASA contract NAS5-26555. This research has also made use of the NASA/IPAC Extragalactic Database (NED) which is operated by the Jet Propulsion Laboratory, California Institute of Technology, under contract with the National Aeronautics and Space Administration.

Table 1. Total Sample Modeled AGN Parameters.[1]

Target	NLR Bicone							Host Disk			
	P.A. (°)	i [2] (°)	θ_{min} (°)	θ_{max} (°)	v_{max} (km/s)	z_{max} (pc)	r_t (pc)	*P.A.* (°)	i [3] (°)	Disk Ref.	β [4] (°)
Circinus	-52	25 (NW)	36	41	300	35	9	30	65	1	7
Mrk 3	89	05 (NE)	—	51	800	270	80	129	64	9	52
Mrk 34	-32	25 (SE)	30	40	1500	1750	1000	65	30	2	85
Mrk 78	65	30 (SW)	10	35	1200	3200	700	84	55	2	87
Mrk 279	-24	55 (SE)	59	62	1800	300	250	33	56	3,4	86
Mrk 573	-36	30 (NW)	51	53	400	1200	800	103	30	3,2	44
Mrk 1066	-41	10 (NW)	15	25	900	400	80	90	54	3	45
NGC 1068	30	05 (NE)	20	40	2000	400	140	115	40	8	45
NGC 1667	55	18 (NW)	45	58	300	100	60	5	39	4	46
NGC 3227	30	75 (SW)	40	55	500	200	100	-31	63	2,5	76
NGC 3783	-20	75 (SE)	45	55	130	110	32	-15	35	6	38
NGC 4051	80	78 (NE)	10	25	550	175	52	50	05	6	15
NGC 4151	60	45 (SW)	15	33	800	400	96	33	20	7	39
NGC 4507	-37	43 (NW)	30	50	1000	200	90	65	28	2	12
NGC 5506	22	10 (SW)	10	40	550	220	65	-89	76	3	32
NGC 5643	80	25 (SE)	50	55	500	285	70	136	30	3	42
NGC 7674	-63	30 (NW)	35	40	1000	700	200	76	40	2	42

[1]Inclination direction (e.g. NW, SE, etc.) specifies which end of the NLR bicone is inclined out of the plane of the sky toward Earth

[2]Inclination of 0° corresponds to an edge-on orientation

[3]Inclination of 0° corresponds to an face-on orientation

[4]Angle between the NLR bicone axis and the normal to the host galaxy disk

References: (1) Freeman et al. (1977), (2) Schmitt & Kinney (2000), (3) Kinney et al. (2000), (4) NED, (5) Xilouris & Papadakis (2002), (6) Hicks et al. (2009), (7) Das et al. (2005), (8) Das et al. (2006), (9) Crenshaw et al. (2010a)

Table 2. Physical properties of modeled AGN sample

Target	Type	log(L_{Bol}) erg s^{-1}	Ref.	log(M_{BH}) $M_\odot$	Ref.	L/L_{edd}	N_H $\times 10^{22}$ cm^{-2}	Ref.	$F_{5.5\mu m}$ (W cm^{-2} μm^{-1})	$F_{30\mu m}$ (W cm^{-2} μm^{-1})	Ref.	Hβ FWHM [1] km s^{-1}	Ref.	log(M_{H_2}) $M_\odot$	Ref.
Circinus	2	42.08	1	6.23	5	0.01	430^{+40}_{-70}	13	—	—	—	—	—	6.30	30
Mrk 3	2	44.54	2	8.65	2	0.01	136^{+3}_{-4}	14	$1.08\pm0.08 \times 10^{-18}$	$8.96\pm0.11 \times 10^{-19}$	26	—	—	—	—
Mrk 34	2	46.13	3	—	–	—	>100	15	$2.75\pm0.17 \times 10^{-19}$	$1.85\pm0.02 \times 10^{-19}$	26	—	—	—	—
Mrk 78	2	44.59	2	7.87	2	0.04	57.5±5.8	16	$3.53\pm0.19 \times 10^{-19}$	$2.10\pm0.02 \times 10^{-19}$	26	—	—	—	—
Mrk 279	1	45.04	3	7.54	6	0.25	>0.034	17	$7.47\pm0.26 \times 10^{-19}$	$1.35\pm0.03 \times 10^{-19}$	26	5411	28	—	—
Mrk 573	2	44.44	2	7.28	2	0.11	>100	18	$7.45\pm0.18 \times 10^{-19}$	$2.58\pm0.04 \times 10^{-19}$	26	—	—	—	—
Mrk 1066	2	44.55	2	7.01	2	0.27	>100	19	$7.45\pm0.70 \times 10^{-19}$	$1.10\pm0.007 \times 10^{-18}$	26	—	—	—	—
NGC 1068	2	44.98	2	6.93	7	0.44	>1000	20	—	—	—	—	—	7.36	31
NGC 1667	2	44.69	2	7.88	2	0.05	>100	21	$7.50\pm3.50 \times 10^{-19}$	$2.22\pm0.06 \times 10^{-19}$	27	—	—	—	—
NGC 3227	1	43.86	2	6.88	8	0.01	0.35±0.18	22	$1.42\pm0.07 \times 10^{-18}$	$6.52\pm0.07 \times 10^{-19}$	26	3823	26	7.31	32
NGC 3783	1	44.59	2	7.47	6	0.05	3.6±0.5	17	$2.37\pm0.13 \times 10^{-18}$	$7.07\pm0.13 \times 10^{-19}$	26	2612	26	6.47	32
NGC 4051	1	43.56	2	6.24	9	0.17	2.1±1.1	17	$2.09\pm0.16 \times 10^{-18}$	$4.13\pm0.04 \times 10^{-19}$	27	1170	29	6.70	32
NGC 4151	1	43.73	2	7.66	10	0.03	9.4±2.8	17	$6.23\pm0.30 \times 10^{-18}$	$1.39\pm0.03 \times 10^{-18}$	26	6421	28	7.15	32
NGC 4507	2	42.92	1	6.13	11	0.05	$43.9^{+5.4}_{-5.7}$	23	$2.09\pm0.10 \times 10^{-18}$	$5.50\pm0.05 \times 10^{-19}$	26	—	—	—	—
NGC 5506	2	44.05	1	6.88	11	0.12	3.7±0.8	24	—	—	—	—	—	—	—
NGC 5643	2	43.98	1	6.79	11	0.12	70.7^{+30}_{-10}	25	$4.73\pm0.46 \times 10^{-19}$	$1.01\pm0.004 \times 10^{-18}$	26	—	—	—	—
NGC 7674	2	45.00	4	7.58	12	0.27	>1000	21	$1.87\pm0.26 \times 10^{-18}$	$6.10\pm0.05 \times 10^{-19}$	27	—	—	—	—

[1] Hβ FWHM values gathered for Seyfert 1s only.

References: (1) Meléndez et al. 2008, (2) Woo & Urry 2002 and references therein, (3) Heckman et al. 2005, (4) Malaguti et al. 1998,, (5) Greenhill et al. 2003, (6) Peterson et al. 2004, (7) Lodato & Bertin 2003, (8) Denney et al. 2010, (9) Denney et al. 2009, (10) Bentz et al. 2006, (11) Gu et al. 2006, (12) Bian & Gu 2007, (13) Matt et al. 1999, (14) Bianchi et al. 2005a, (15) Greenhill et al. 2008, (16) Gilli et al. 2010, (17) Crenshaw & Kraemer 2012, (18) Shu et al. 2007, (19) Risaliti et al. 1999, (20) Matt et al. 2004b, (21) Bianchi et al. 2005b, (22) Markowitz et al. 2009, (23) Matt et al. 2004a, (24) Risaliti et al. 2002, (25) Guainazzi et al. 2004, (26) This work, (27) Deo et al. 2009, (28) Vestergaard & Peterson 2006, (29) Grupe et al. 2004, (30) Müller Sánchez et al. 2006, (31) Müller Sánchez et al. 2009, (32)Hicks et al. 2009

Table 3. Correlations between modeled/observed AGN properties

Correlation	r	N	$P_c(r, N)$
i vs N_H	.86	15	0.000039
z_{max} vs r_t	.82	16	0.00010
i vs IR Color[1]	-.74	15	0.0016
i vs Hβ FWHM	.94	5	0.017
r_t vs L_{Bol}	.56	16	0.024
v_{max} vs L_{Bol}	.52	16	0.039
z_{max} vs L_{Bol}	.43	16	0.096
β angle vs N_H	-.33	16	0.21
v_{max} vs r_t	.32	16	0.23
v_{max} vs z_{max}	.31	16	0.24
v_{max} vs M_{H_2}	.53	4	0.47
θ_{max} vs L_{Bol}	.17	16	0.53
v_{max} vs θ_{max}	-.13	16	0.63
θ_{max} vs M_{H_2}	.25	4	0.75

[1] $F_{5.5\mu m}/F_{30\mu m}$

REFERENCES

Antonucci, R. 1993, ARA&A, 31, 473

Antonucci, R. R. J., & Miller, J. S. 1985, ApJ, 297, 621

Bentz, M. C. et al. 2006, ApJ, 651, 775

Bian, W., & Gu, Q. 2007, ApJ, 657, 159

Bianchi, S., Guainazzi, M., Matt, G., Chiaberge, M., Iwasawa, K., Fiore, F., & Maiolino, R. 2005a, A&A, 442, 185

Bianchi, S., Miniutti, G., Fabian, A. C., & Iwasawa, K. 2005b, MNRAS, 360, 380

Collin, S., Kawaguchi, T., Peterson, B. M., & Vestergaard, M. 2006, A&A, 456, 75

Crenshaw, D. M., & Kraemer, S. B. 2000, ApJ, 532, L101

——. 2001, ApJ, 562, L29

——. 2012, ApJ, 753, 75

Crenshaw, D. M., Kraemer, S. B., Boggess, A., Maran, S. P., Mushotzky, R. F., & Wu, C.-C. 1999, ApJ, 516, 750

Crenshaw, D. M., Kraemer, S. B., & George, I. M. 2003, ARA&A, 41, 117

Crenshaw, D. M. et al. 2000, AJ, 120, 1731

Crenshaw, D. M., Kraemer, S. B., Schmitt, H. R., Jaffé, Y. L., Deo, R. P., Collins, N. R., & Fischer, T. C. 2010a, AJ, 139, 871

Crenshaw, D. M., Schmitt, H. R., Kraemer, S. B., Mushotzky, R. F., & Dunn, J. P. 2010b, ApJ, 708, 419

Das, V. et al. 2005, AJ, 130, 945

Das, V., Crenshaw, D. M., Kraemer, S. B., & Deo, R. P. 2006, AJ, 132, 620

Denney, K. D. 2012, ApJ, 759, 44

Denney, K. D. et al. 2010, ApJ, 721, 715

——. 2009, ApJ, 702, 1353

Deo, R. P., Richards, G. T., Crenshaw, D. M., & Kraemer, S. B. 2009, ApJ, 705, 14

Elitzur, M. 2012, ApJ, 747, L33

Fischer, T. C., Crenshaw, D. M., Kraemer, S. B., & Schmitt, H. R. 2013, ArXiv e-prints

Fischer, T. C., Crenshaw, D. M., Kraemer, S. B., Schmitt, H. R., Mushotsky, R. F., & Dunn, J. P. 2011, ApJ, 727, 71

Fischer, T. C., Crenshaw, D. M., Kraemer, S. B., Schmitt, H. R., & Trippe, M. L. 2010, AJ, 140, 577

Freeman, K. C., Karlsson, B., Lynga, G., Burrell, J. F., van Woerden, H., Goss, W. M., & Mebold, U. 1977, A&A, 55, 445

Friedrich, S., Davies, R. I., Hicks, E. K. S., Engel, H., Müller-Sánchez, F., Genzel, R., & Tacconi, L. J. 2010, A&A, 519, A79

Fritz, J., Franceschini, A., & Hatziminaoglou, E. 2006, MNRAS, 366, 767

Gaskell, C. M. 2000, New A Rev., 44, 563

——. 2009, New A Rev., 53, 140

Gilli, R., Vignali, C., Mignoli, M., Iwasawa, K., Comastri, A., & Zamorani, G. 2010, A&A, 519, A92

Greenhill, L. J. et al. 2003, ApJ, 590, 162

Greenhill, L. J., Tilak, A., & Madejski, G. 2008, ApJ, 686, L13

Grupe, D., Wills, B. J., Leighly, K. M., & Meusinger, H. 2004, AJ, 127, 156

Gu, Q., Melnick, J., Cid Fernandes, R., Kunth, D., Terlevich, E., & Terlevich, R. 2006, MNRAS, 366, 480

Guainazzi, M., Bianchi, S., Matt, G., Dadina, M., Kaastra, J., Malzac, J., & Risaliti, G. 2010, MNRAS, 406, 2013

Guainazzi, M., Rodriguez-Pascual, P., Fabian, A. C., Iwasawa, K., & Matt, G. 2004, MNRAS, 355, 297

Heckman, T. M., Kauffmann, G., Brinchmann, J., Charlot, S., Tremonti, C., & White, S. D. M. 2004, ApJ, 613, 109

Heckman, T. M., Ptak, A., Hornschemeier, A., & Kauffmann, G. 2005, ApJ, 634, 161

Hicks, E. K. S., Davies, R. I., Malkan, M. A., Genzel, R., Tacconi, L. J., Müller Sánchez, F., & Sternberg, A. 2009, ApJ, 696, 448

Khachikian, E. Y., & Weedman, D. W. 1974, ApJ, 192, 581

Kinney, A. L., Schmitt, H. R., Clarke, C. J., Pringle, J. E., Ulvestad, J. S., & Antonucci, R. R. J. 2000, ApJ, 537, 152

Kraemer, S. B. et al. 2012, ApJ, 751, 84

Kraemer, S. B., Trippe, M. L., Crenshaw, D. M., Meléndez, M., Schmitt, H. R., & Fischer, T. C. 2009, ApJ, 698, 106

Lebouteiller, V., Barry, D. J., Spoon, H. W. W., Bernard-Salas, J., Sloan, G. C., Houck, J. R., & Weedman, D. W. 2011, ApJS, 196, 8

Lodato, G., & Bertin, G. 2003, A&A, 398, 517

Maiolino, R., & Rieke, G. H. 1995, ApJ, 454, 95

Malaguti, G. et al. 1998, A&A, 331, 519

Markowitz, A., Reeves, J. N., George, I. M., Braito, V., Smith, R., Vaughan, S., Arévalo, P., & Tombesi, F. 2009, ApJ, 691, 922

Matt, G., Bianchi, S., D'Ammando, F., & Martocchia, A. 2004a, A&A, 421, 473

Matt, G., Bianchi, S., Guainazzi, M., & Molendi, S. 2004b, A&A, 414, 155

Matt, G. et al. 1999, A&A, 341, L39

Meléndez, M., Kraemer, S. B., Schmitt, H. R., Crenshaw, D. M., Deo, R. P., Mushotzky, R. F., & Bruhweiler, F. C. 2008, ApJ, 689, 95

Müller Sánchez, F., Davies, R. I., Eisenhauer, F., Tacconi, L. J., Genzel, R., & Sternberg, A. 2006, A&A, 454, 481

Müller Sánchez, F., Davies, R. I., Genzel, R., Tacconi, L. J., Eisenhauer, F., Hicks, E. K. S., Friedrich, S., & Sternberg, A. 2009, ApJ, 691, 749

Müller-Sánchez, F., Prieto, M. A., Hicks, E. K. S., Vives-Arias, H., Davies, R. I., Malkan, M., Tacconi, L. J., & Genzel, R. 2011, ApJ, 739, 69

Murray, N., & Chiang, J. 1997, ApJ, 474, 91

Nagar, N. M., Oliva, E., Marconi, A., & Maiolino, R. 2002, A&A, 391, L21

Osterbrock, D. E. 1978, Proceedings of the National Academy of Science, 75, 540

Pancoast, A. et al. 2012, ApJ, 754, 49

Peterson, B. M. 1997, An Introduction to Active Galactic Nuclei (Cambridge University Press)

Peterson, B. M. et al. 2004, ApJ, 613, 682

Ramos Almeida, C. et al. 2009, ApJ, 702, 1127

Risaliti, G., Elvis, M., & Nicastro, F. 2002, ApJ, 571, 234

Risaliti, G., Maiolino, R., & Salvati, M. 1999, ApJ, 522, 157

Roth, N., Kasen, D., Hopkins, P. F., & Quataert, E. 2012, ApJ, 759, 36

Ruiz, J. R., Crenshaw, D. M., Kraemer, S. B., Bower, G. A., Gull, T. R., Hutchings, J. B., Kaiser, M. E., & Weistrop, D. 2001, AJ, 122, 2961

Schmitt, H. R., Donley, J. L., Antonucci, R. R. J., Hutchings, J. B., & Kinney, A. L. 2003, ApJS, 148, 327

Schmitt, H. R., & Kinney, A. L. 2000, ApJS, 128, 479

Shu, X. W., Wang, J. X., Jiang, P., Fan, L. L., & Wang, T. G. 2007, ApJ, 657, 167

Stalevski, M., Fritz, J., Baes, M., Nakos, T., & Popović, L. Č. 2012, MNRAS, 420, 2756

Tombesi, F., Cappi, M., Reeves, J. N., Nemmen, R. S., Braito, V., Gaspari, M., & Reynolds, C. S. 2013, MNRAS, 430, 1102

Tremaine, S. et al. 2002, ApJ, 574, 740

Trippe, M. L., Crenshaw, D. M., Deo, R. P., Dietrich, M., Kraemer, S. B., Rafter, S. E., & Turner, T. J. 2010, ApJ, 725, 1749

Turner, T. J., & Miller, L. 2009, A&A Rev., 17, 47

Vestergaard, M., & Peterson, B. M. 2006, ApJ, 641, 689

Walsh, J. L., Barth, A. J., Ho, L. C., Filippenko, A. V., Rix, H.-W., Shields, J. C., Sarzi, M., & Sargent, W. L. W. 2008, AJ, 136, 1677

Winter, L. M., Mushotzky, R. F., Reynolds, C. S., & Tueller, J. 2009, ApJ, 690, 1322

Woo, J.-H., & Urry, C. M. 2002, ApJ, 579, 530

Xilouris, E. M., & Papadakis, I. E. 2002, A&A, 387, 441

Yan, R., & Blanton, M. R. 2012, ApJ, 747, 61

Zeng, J. 2009, PhD thesis, University of Maryland, Baltimore County

This preprint was prepared with the AAS LaTeX macros v5.2.

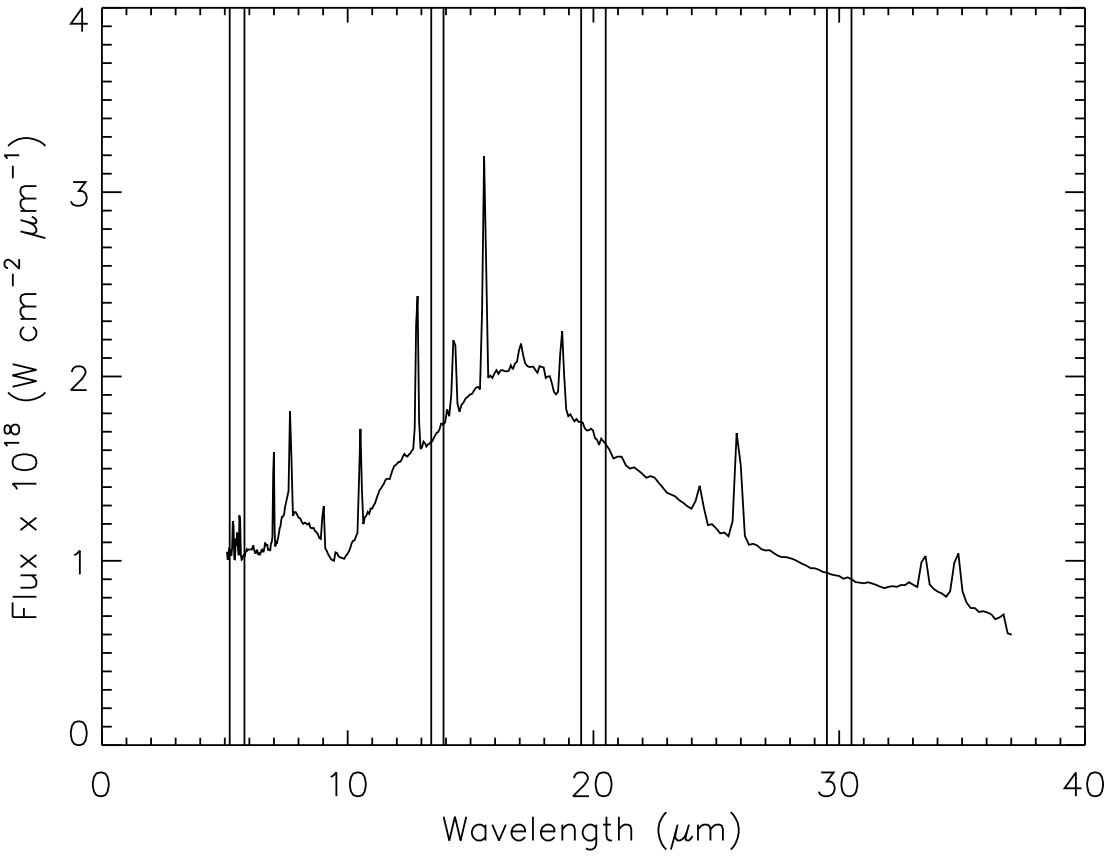

Fig. 1.— Mid-IR *Spitzer* spectrum of Mrk 3 gathered from CASSIS. Vertical lines from left to right denote 5.5μm, 13.7μm, 20μm, and 30μm flux bins.

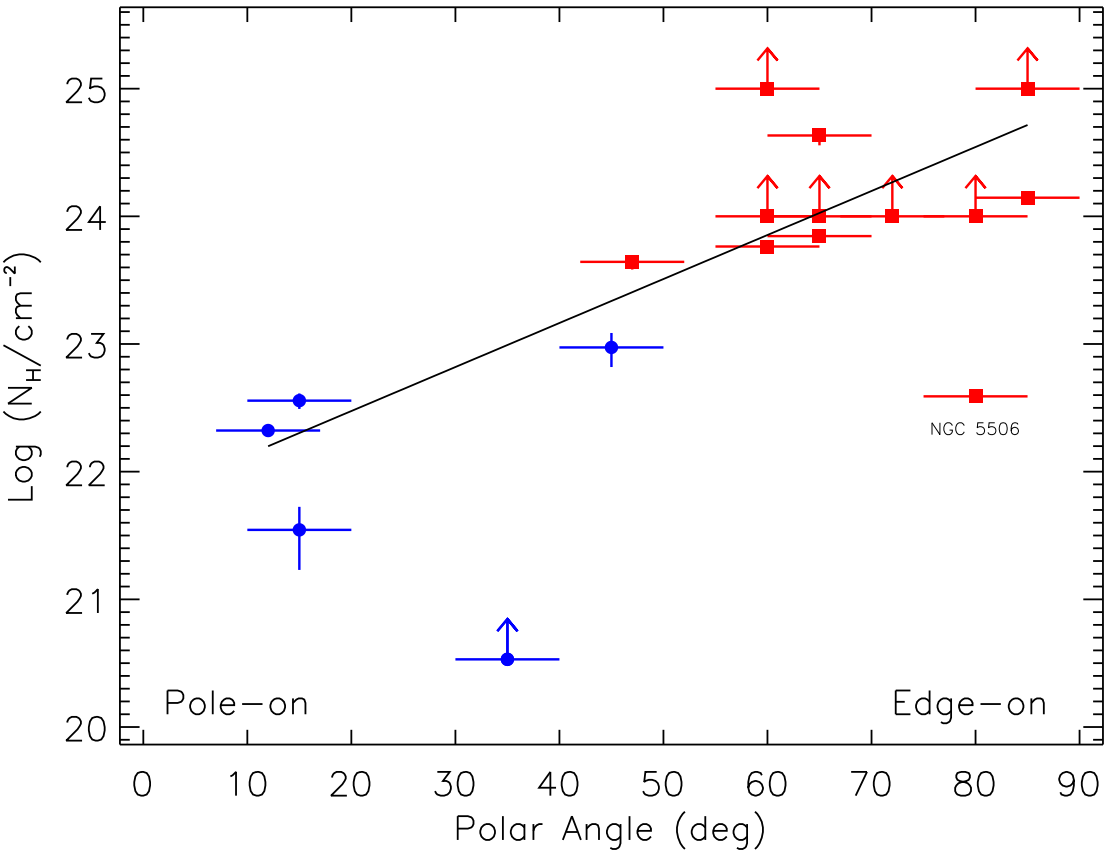

Fig. 2.— Inclination from our line of sight to the bicone axis versus the x-ray column density (ionized for Seyfert 1s, cold for Seyfert 2s), where a continuous trend can be seen between Seyfert 1s and 2s. Seyfert 1s are designated as blue circles, Seyfert 2s are designated as red squares. Points with arrows show lower limits of column densities.

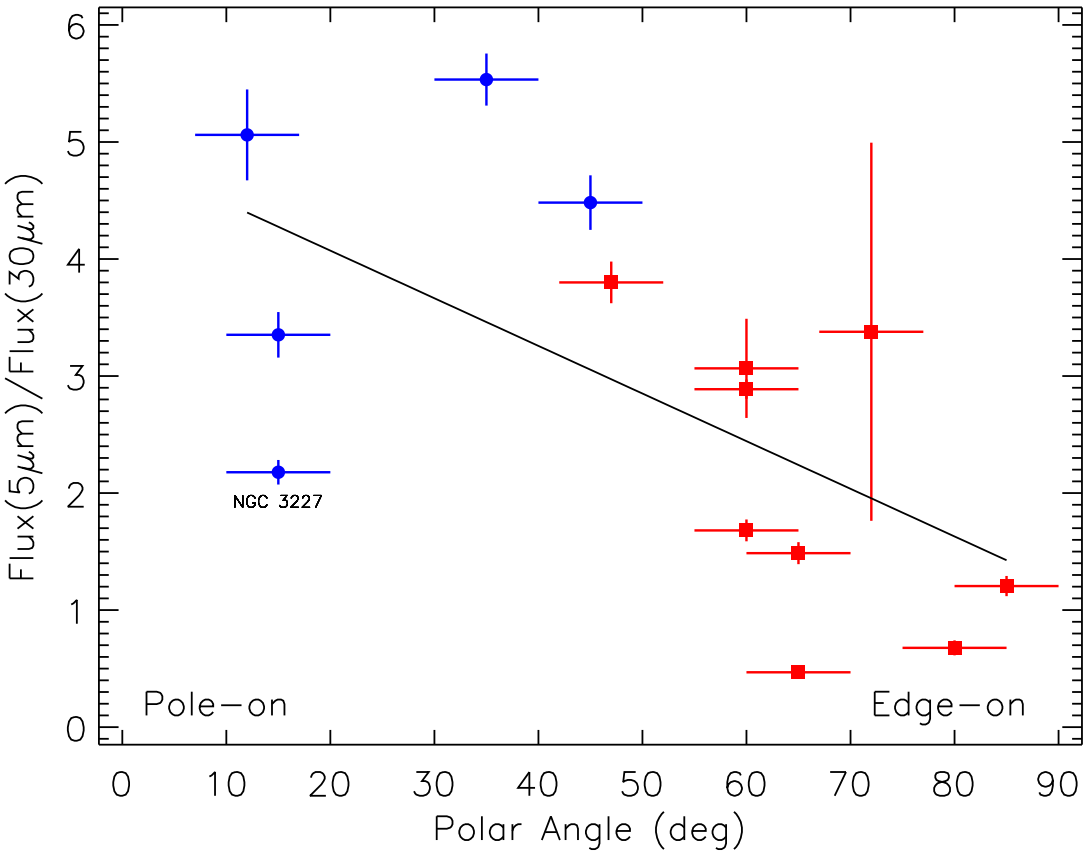

Fig. 3.— Inclination from our line of sight to the bicone axis versus AGN mid-IR color ($F_{5.5\mu m}/F_{30\mu m}$). Seyfert 1s are designated as blue circles, Seyfert 2s are designated as red squares.

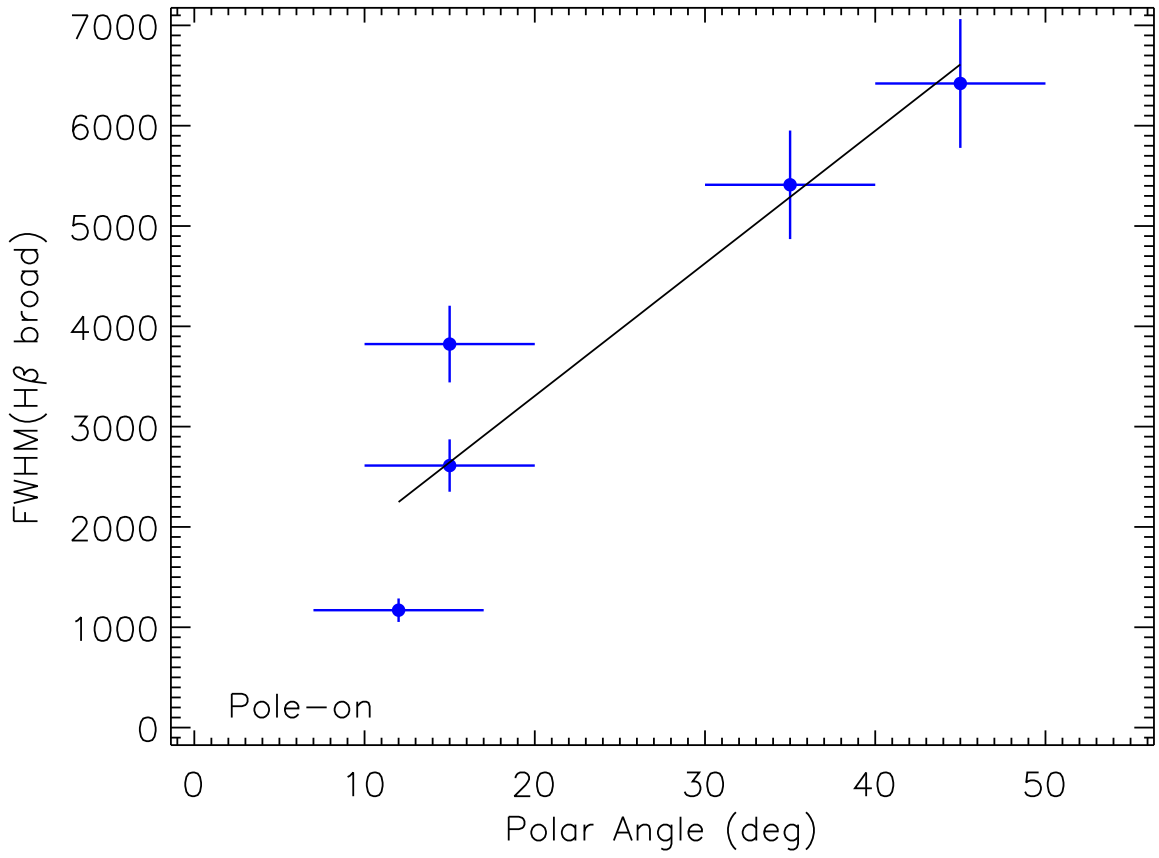

Fig. 4.— Inclination from our line of sight to the bicone axis versus Hβ FWHM for modeled Seyfert 1s.

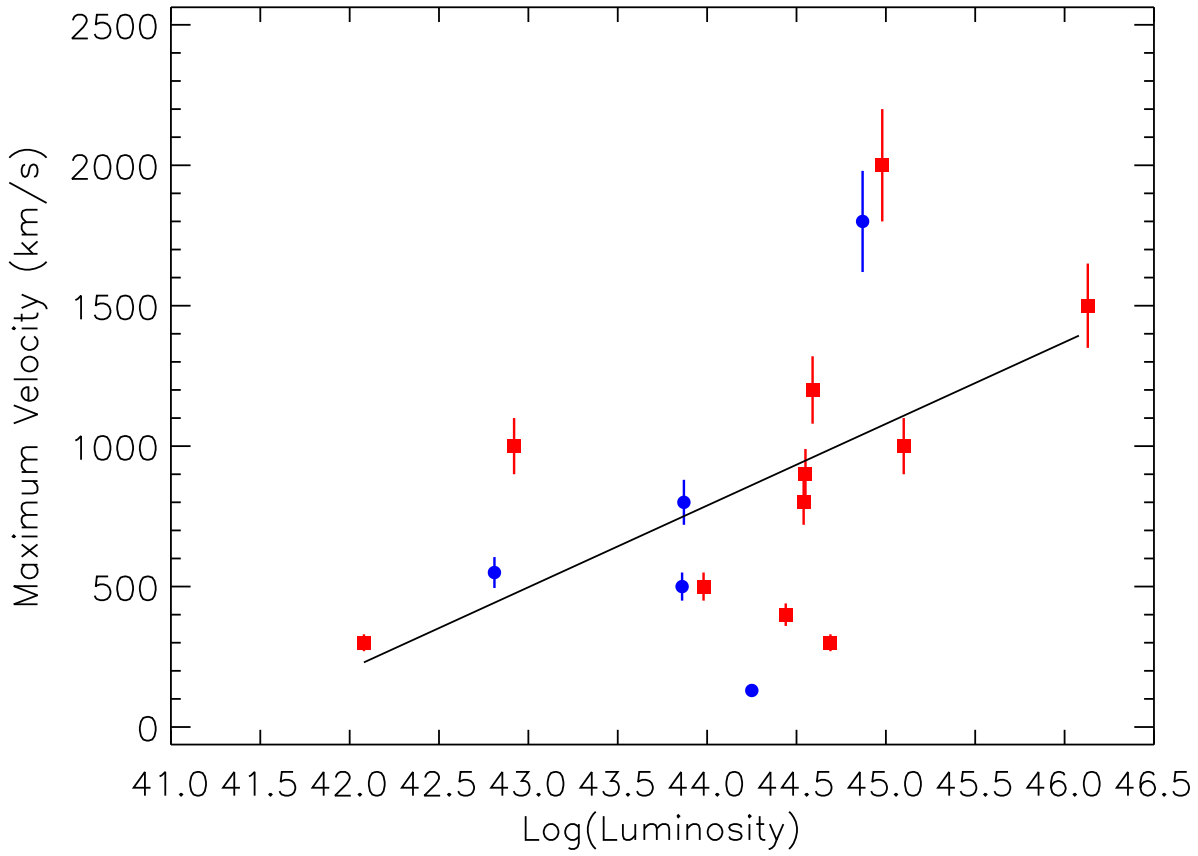

Fig. 5.— Bolometric luminosity versus maximum deprojected outflow velocity of the NLR for each of our modeled targets. Seyfert 1s are designated as blue circles, Seyfert 2s are designated as red squares. Luminosity are uncertain by approximately a factor of two. Modeled parameters contain uncertainties of approximately 10% the modeled value.

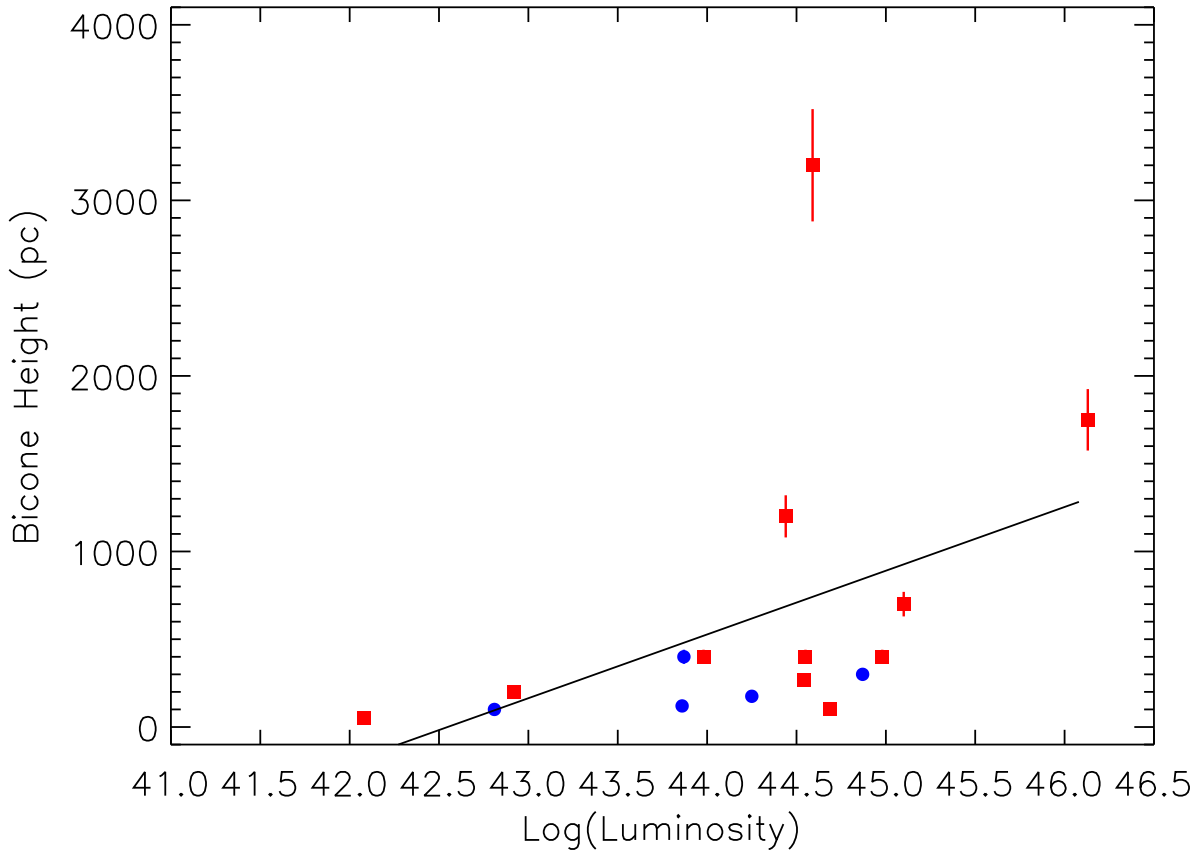

Fig. 6.— Bolometric luminosity versus NLR bicone height for each of our modeled targets. Seyfert 1s are designated as blue circles, Seyfert 2s are designated as red squares. Luminosity are uncertain by approximately a factor of two. Modeled parameters contain uncertainties of approximately 10% the modeled value.

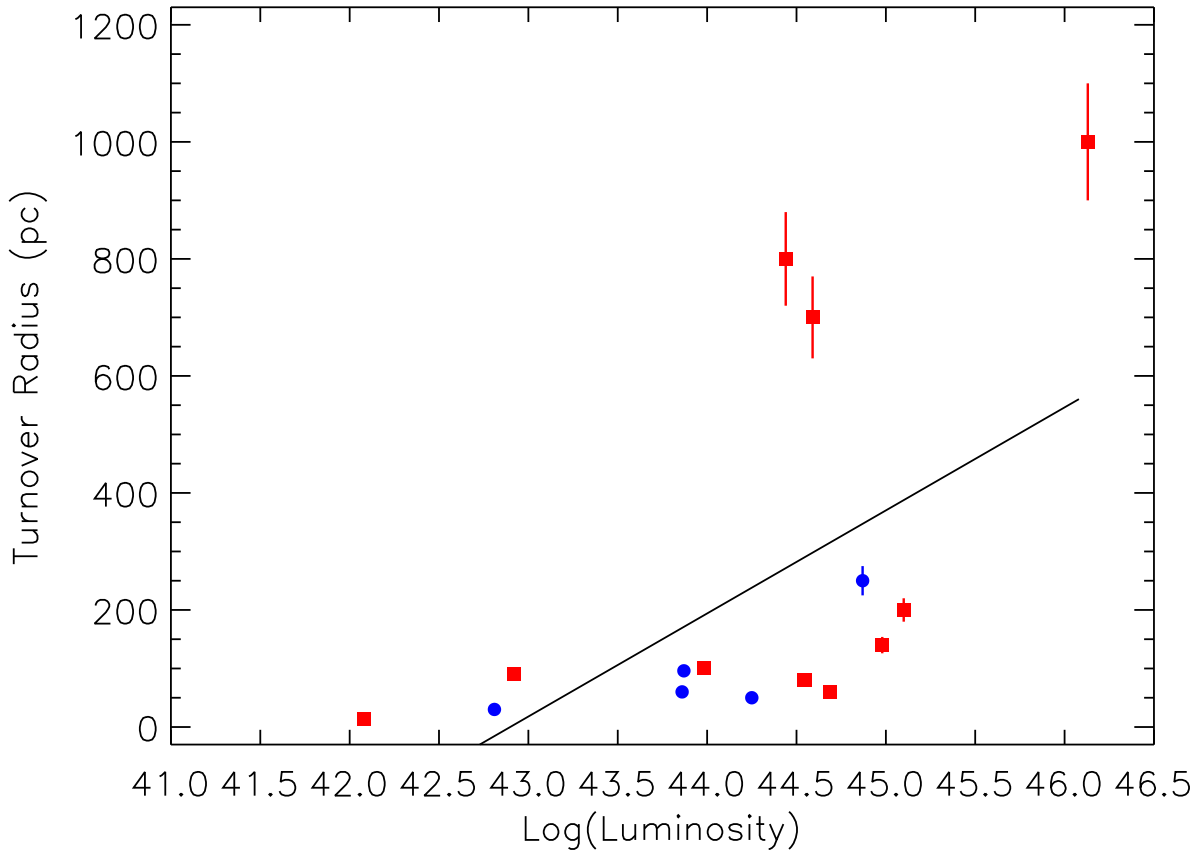

Fig. 7.— Bolometric Luminosity versus kinematic turnover radius for each of our modeled targets. Seyfert 1s are designated as blue circles, Seyfert 2s are designated as red squares. Luminosity are uncertain by approximately a factor of two. Modeled parameters contain uncertainties of approximately 10% the modeled value.

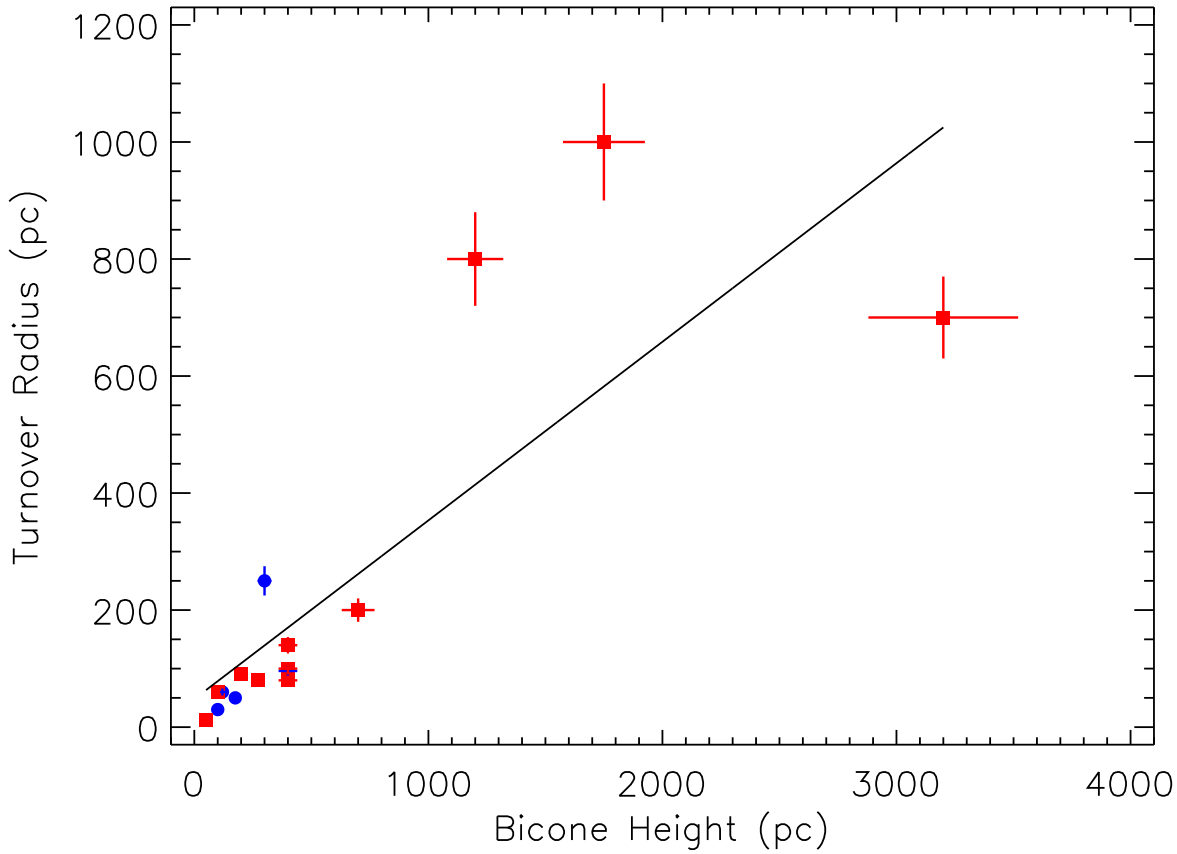

Fig. 8.— NLR bicone height versus kinematic turnover radius for each of our modeled targets. Seyfert 1s are designated as blue circles, Seyfert 2s are designated as red squares. Modeled parameters contain uncertainties of approximately 10% the modeled value.